Berkelium–Carbon Bonding in a Tetravalent Berkelocene

Dominic R. Russo,[1,2‡] Alyssa N. Gaiser,[1‡] Amy N. Price,[1,2‡] Dumitru-Claudiu Sergentu,[3,4‡] Jennifer N. Wacker,[1] Nicholas Katzer,[1,2] Appie A. Peterson,[1] Jacob A. Branson,[1,2] Xiaojuan Yu,[5] Sheridon N. Kelly,[1,2] Erik T. Ouellette,[1,2] John Arnold,[1,2] Jeffrey R. Long,[1,2,6,7] Wayne W. Lukens Jr,[1] Simon J. Teat,[1] Rebecca J. Abergel,[1,2,8]* Polly L. Arnold,[1,2]* Jochen Autschbach,[5]* Stefan G. Minasian[1]*

[1] Lawrence Berkeley National Laboratory, Berkeley, CA 94720, USA.
[2] Department of Chemistry, University of California, Berkeley, CA 94720, USA.
[3] Faculty of Chemistry, Alexandru Ioan Cuza University of Iași, Iași 700506, Romania.
[4] RA-03 (RECENT AIR) Laboratory, Alexandru Ioan Cuza University of Iași, Iași 700506, Romania.
[5] Department of Chemistry, University of Buffalo; Buffalo, New York, 14260, USA.
[6] Department of Chemical and Biomolecular Engineering, University of California, Berkeley, CA 94720, USA.
[7] Department of Materials Science and Engineering, University of California, Berkeley, CA 94720, USA.
[8] Department of Nuclear Engineering, University of California, Berkeley, CA 94720, USA.
‡ These authors contributed equally
* To whom correspondence should be addressed; E-mail: rjabergel@lbl.gov, pla@lbl.gov, jochena@buffalo.edu, sgminasian@lbl.gov.

Abstract

Interest in actinide–carbon bonds has persisted since actinide organometallics were first targeted for isotope separation during the Manhattan Project. Sandwich complexes with cyclooctatetraenide ligands have been used extensively to form tetravalent actinide compounds, "actinocenes," from thorium through plutonium. These complexes have been pivotal in the development of electronic structure models used throughout inorganic chemistry. The isolation and structural characterization of transplutonium organometallics is extremely challenging due to limited isotope inventories, a scarcity of suitable laboratory infrastructure, and intrinsic difficulties with the anaerobic conditions required. Herein, we show that berkelium–carbon bonds can be stabilized in an organometallic "berkelocene" complex. Metal–ligand bonding involves the berkelium 5f orbitals in covalent overlap; however, charge transfer from the ligands is reduced to maximize contributions from the stable, half-filled $5f^7$ configuration of tetravalent berkelium.

One-Sentence Summary

A metallocene complex featuring the first Bk^{4+}–C bonds was isolated and characterized.

Introduction

Modern organometallic chemistry can be traced to the elucidation of a "sandwich" structure for ferrocene, $Fe(Cp)_2$ ($Cp = C_5R_5^-$), in the early 1950s by Wilkinson and Fischer (*1, 2*). These reports nearly coincided with the discovery of two actinide elements, berkelium (Bk) and californium (Cf), which were reported by Seaborg and coworkers in 1950 (*3, 4*). However, for many years the fields of organometallic and actinide chemistry followed essentially separate trajectories. In contrast to $Fe(Cp)_2$, the first Cp complexes of actinides were highly reactive and air-sensitive (*5*), and actinide alkyl and carbonyl complexes – which are ubiquitous for d-block metals – were far too unstable to isolate (*6*). Interest in organoactinide chemistry was reignited with the synthesis and structural characterization of uranocene, $U(COT)_2$ ($COT = C_8H_8^{2-}$) in the late 1960s by Streitwieser, Raymond and coworkers (*7, 8*). By 1976, all the actinocenes, of the form $An(COT)_2$ (An = actinide), from Th through Pu (*9-11*) as well as the lanthanide analog with Ce, cerocene (*12*), were characterized. Save for some early microscale studies, (*13, 14*) the organometallic chemistry of transplutonium elements remained undeveloped until recently. The isolation and characterization of the trivalent Am and Cf complexes with Cp ligands, reported by Gaunt and coworkers in 2019 and 2021, respectively, constituted the first structural verifications of An–C bonds for elements beyond Pu (*15, 16*).

The tetravalent COT actinocenes have played a leading role in spectroscopic and theoretical investigations of actinide covalency because of their characteristic highly symmetric, homoleptic ligand environment (*17-22*). The high symmetry restricts hybridization of 5f with 6d orbitals and at the same time supports 5f- and 6d-orbital mixing with the ligand frontier orbitals to form molecular orbitals of σ, π, δ, and φ symmetry. Compared to trivalent complexes, the greater metal charge found in tetravalent actinocenes stabilizes the An 5f- and 6d-orbitals, thereby reducing the difference in energy with ligand-orbitals and potentially enhancing covalent mixing (*20*). Despite considerable synthetic, spectroscopic, and theoretical progress, it remains unknown whether our understanding of covalent actinide bonding derived from the chemistry of early actinides can be applied to the transplutonium elements (*23-25*). In targeting such an actinocene for synthesis, we noted that the tetravalent oxidation state is uniquely accessible for Bk compared with the neighboring elements, due to the stability of the associated half-filled, $5f^7$ electronic configuration (*26, 27*). Herein, we describe our efforts to develop the organometallic chemistry of tetravalent Bk, leading to the discovery of the first tetravalent Bk actinocene, or "berkelocene."

Results and Discussion

Synthesis. Developing high-valent Bk organometallic chemistry required overcoming several unique scientific and technical challenges because of the scarcity and high radioactivity of its most readily available isotope, ^{249}Bk ($t_{1/2}$ = 330(4) days). Recent progress in molecular transuranium synthetic chemistry, however, has provided the tools necessary to explore the synthetic chemistry of Bk (*24, 25*). Synthetic protocols were developed that are compatible with the air- and moisture-sensitivity typical of organometallics and reproducible even at ultra-small scales while ensuring responsible stewardship of the precious and hazardous isotope. For example, the entire experimental process, from the first synthetic step through to isolation and characterization of the final product, was designed to be achievable within a ~48 h time frame. Short-duration experiments were necessary to avoid potential product decomposition and crystal disintegration due to radiolysis and in-growth of ^{249}Cf, the primary daughter of ^{249}Bk. Additionally, the synthesis had

to be resilient to ^{249}Cf impurities present in the starting material (~0.2 mg or ~0.8 μmol of Cf^{3+}) while also accommodating excess reagents left over from preceding synthetic steps. Crucially, no solvents or reagents could be used that would impede future Bk reprocessing or prevent proper disposal.

Synthetic protocols were designed for 0.5 mg (2 μmol of total metal content) scale reactions with all details of the procedure optimized in advance using Ce as a non-radioactive and abundant lanthanide surrogate to demonstrate reproducibility. Chemical oxidation (*26*) and electrolytic experiments have shown that the Bk^{4+}/Bk^{3+} reduction potential and its sensitivity to the surrounding ligand environment are comparable to that of Ce^{4+}/Ce^{3+} (*28-30*). In addition to unsubstituted COT, conditions for small-scale cerocene syntheses were optimized using four substituted COT ligands with different solubilizing and electron-donating characteristics. The hdcCOT ligand (hdcCOT = hexahydrodicyclopenta[8]annulene) consistently provided the $Ce(hdcCOT)_2$ complex when using ~0.5 mg of Ce, and hence hdcCOT was selected for subsequent Bk experiments (see Supplementary Materials) (*31, 32*). Tetravalent cerocenes are best synthesized by oxidation of a trivalent cerium complex (*33, 34*), so a variety of organic oxidants were also tested. Ultimately, chlorotriphenylmethane (Ph_3CCl) was selected as an oxidant owing to waste management constraints (*vide supra*).

The anhydrous precursor $BkCl_3(DME)_n$ (DME = 1,2-dimethoxyethane) was prepared as an off-white solid by treating a pale-green sample of hydrated $BkCl_3$ with Me_3SiCl in DME, Fig. 1 (*23, 25*). Following evaporation, the solid residue was suspended in tetrahydrofuran (THF) and 2.5 equivalents of K_2hdcCOT were added to form a yellow-orange solution. No color change was observed after ~16 h of stirring and the putative trivalent product, "K[Bk(hdcCOT)$_2$]," appeared to remain in solution. Addition of a THF solution containing 3.5 equivalents of Ph_3CCl resulted in an immediate color change to indigo. Following work-up, evaporation of a *n*-pentane solution yielded indigo crystals that were analyzed by single crystal X-ray diffraction, confirming the formation of $Bk(hdcCOT)_2$.

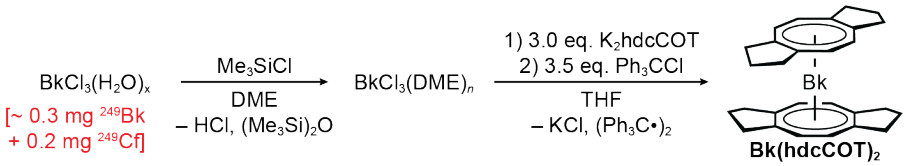

Fig. 1. Synthesis of a tetravalent Bk metallocene, Bk(hdcCOT)$_2$.

Crystallography

The complex crystallizes in the space group $P\bar{1}$ with the Bk atom positioned on an inversion center and a $hdcCOT_{cent(1)}$–Bk(1)–$hdcCOT_{cent(2)}$ angle of 178.3(5)° (Fig. 2A and 2B). The two hdcCOT rings are rotated about the Bk–centroid axis to form a pseudo-D_2 symmetry structure, with all four carbocyclic cyclopentane rings adopting a boat-like, all *endo*-conformation (i.e., bending towards the Bk atom). The average torsion angle between the observed pseudo-D_2 conformation and a D_{2h} (eclipsed) confirmation is 55(2)° (χ_2, Fig 2B). In contrast, $Ce(hdcCOT)_2$ (see Supplemental Materials) and other $An(hdcCOT)_2$ complexes (An = Th, U, Np, Pu) (*35*) crystallize in the space group $P2_1/c$, exhibiting rigorous D_{2h} point symmetry with the two carbocyclic cyclopentane rings adopting a chair-like, *exo-endo* conformation at low temperature. Notably, uranocene adopts a

range of structural conformations depending on the nature of COT ligand substituents (*36-38*), and the potential energy associated with the staggered-to-eclipsed transformation for the *endo* system is computed to be nearly invariant between 0–30° (*vide infra*).

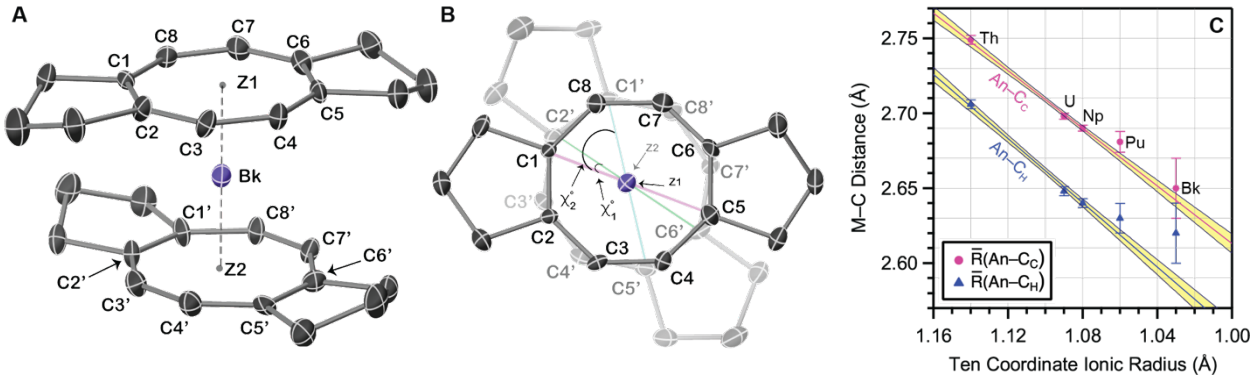

Fig. 2. X-ray Crystallography. (A) Thermal ellipsoid (50%) plot of Bk(hdcCOT)$_2$, viewed from the side and (B) down the centroid—Bk—centroid axis. (C) Plot of the mean An–C distances (Å) in An(hdcCOT)$_2$ complexes (An = Th, U, Np, Pu, Bk) as a function of the 10-coordinate ionic radius of the metal cations. Refer to the supplementary information for details on the calculation of 10-coordinate ionic radii. Error bars are based on the standard deviation in the mean of chemically equivalent distances.

The C–C bond distances in Bk(hdcCOT)$_2$ are between 1.40(2) and 1.42(3) Å, which is typical of C–C distances in both substituted and unsubstituted COT ligands (*31, 39-41*). The Bk–C distances range between 2.60(3) to 2.66(4), and the average Bk–hdcCOT$_{cent}$ distance is 1.88(2) Å. With additional structural data for other An(hdcCOT)$_2$ complexes, the crystal structure of Bk(hdcCOT)$_2$ provides a new opportunity to compare changes in An–C bond lengths across much of the actinide series (Fig. 2C). The central C_8 ring of the hdcCOT ligand has two types of C atoms: those bonded to the carbocyclic rings (C_C) and those bonded to H atoms (C_H). Figure 2C shows that M–C_C distances are typically ~0.02 Å longer than M–C_H distances, which is attributed to differences in the steric environment. Linear fits provide good correlation coefficients (r^2) of 0.956 and 0.992 for the An–C_C and An–C_H data, respectively. Shorter An–C_C and An–C_H distances are observed for metals with smaller ionic radii. The strong linear correlation suggests that the bond metrics may be well rationalized based solely on changes in the metal ionic radii (*42*), however differences in crystallographic disorder, local symmetry, space group, and crystal packing effects cannot be fully ruled out.

UV-Vis Absorption Spectroscopy

Absorption spectra of K$_2$hdcCOT, [K(crypt)][Gd(hdcCOT)$_2$], Ce(hdcCOT)$_2$, and Bk(hdcCOT)$_2$ (Fig. 3A) corroborate the purple-indigo colors observed during synthesis. Intense features are observed in the visible region at 545 and 700 nm for Bk(hdcCOT)$_2$ and at 500 and 600 nm for Ce(hdcCOT)$_2$. As described for Ce(COT)$_2$ (*33, 43*), these bands are assigned to ligand-to-metal charge transfer (LMCT) transitions. By contrast, the analogous $4f^7$ complex, [K(crypt)][Gd(hdcCOT)$_2$], is essentially featureless in this energy regime with its first absorption band occurring at 345 nm and is, spectroscopically, more similar to K$_2$hdcCOT (Fig. S15). The slight increase in energy for the LMCT bands may reflect the higher energy of the Ce 4f orbitals

relative to the Bk 5f orbitals, based on 4th ionization potentials (*44, 45*). Compared to other known Bk(IV) compounds, the lower energy of the LMCT bands for Bk(hdcCOT)$_2$ relative to Bk[3,4,3-LI(1,2-HOPO)] (400 nm) (*46*) and Bk(IO$_3$)$_4$ (450 nm) (*25*) is attributed to the higher energy of the ligand-based C 2p versus O 2p atomic orbitals. Taken together with theory (*vide infra*), these observations and assignments are consistent with a Bk^{4+} organometallic complex.

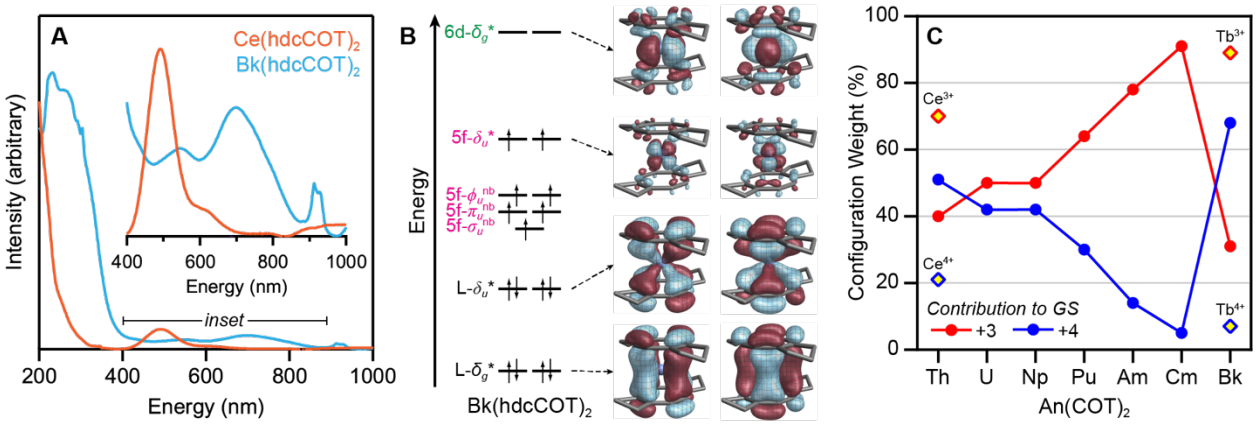

Fig. 3. (**A**) Experimental UV-Vis absorbance spectra of Bk(hdcCOT)$_2$ in *n*-pentane (blue) obtained from the mother liquor solution compared with a spectrum of Ce(hdcCOT)$_2$ in *n*-pentane (orange). The inset shows an expansion of the LMCT region. Experimental determination of extinction coefficients was precluded by the low sample concentration and by the presence of soluble redox byproducts (e.g., Gomberg's dimer and neutral hdcCOT). Absorption features above 400 nm are partially attributed to $Ph_3C^{\bullet}$ and $(Ph_3C^{\bullet})_2$ byproducts formed during the oxidation with Ph_3CCl, which were not removed prior to the measurement (*47*). Sharp features at 913 and 927 nm are characteristic of f-f transitions, which could be associated with Bk(hdcCOT)$_2$ or with small amounts of Bk^{3+} or Cf^{3+} impurities. (**B**) Qualitative valence MO diagram showing the most important metal-ligand bonding interactions and ordering of the nonbonding 5f orbitals from a CAS calculation targeting the ground state. (**C**) Contributions from An^{4+} and An^{3+} configurations to the ground state CAS wavefunctions of D_{8h}-An(COT)$_2$, An = Th to Bk, expressed in an orbital basis with localized δ_u species. Data for Ce(COT)$_2$ and Tb(COT)$_2$ (*48, 49*) are provided for comparison.

Electronic Structure Calculations

Density functional theory (DFT) for isolated Bk(hdcCOT)$_2$ predicts a global minimum structure with D_{2d} symmetry and a completely *endo* conformation of the carbocylic cyclopentanes. At higher energy, within 19 kJ mol^{-1}, are the *endo-exo* and *exo-exo* conformers (Fig. S1A). These structures have Bk–hdcCOT$_{cent}$ and average Bk–C$_{hdcCOT}$ distances of 1.88 and 2.61–2.65 Å, which are in excellent agreement with the experimental data (*vide supra*). The potential energy profile associated with the rotation between the calculated D_{2d} conformer and the experimentally-observed D_{2h} geometry for the endo hdcCOT system is nearly flat between 0° and 30° (Fig. S1B), suggesting that the observed geometry of Bk(hdcCOT)$_2$ in the crystal could easily be due to crystal packing.

Relativistic complete active space (CAS) self-consistent field wavefunction calculations of all possible ligand-field spin states of the $5f^7$ configuration, followed by multireference treatment of the dynamic electron correlation and treatment of spin-orbit coupling (SOC), were performed for Bk(hdcCOT)$_2$ and the experimentally unknown Bk(COT)$_2$. The resulting energy-level scheme (Fig. S1C) shows an $^8S_{7/2}$ ground state, along with ligand-field-split Kramers components of $^6D_{7/2}$ ion parentage around 1.69 eV (corresponding to a photon wavelength of 733 nm). This energy, although somewhat overestimated, matches that of the sharp f-f transitions in the absorption

spectrum at 913 and 927 nm (1.36 and 1.34 eV). Time-dependent DFT calculations of LMCT states (Table S1) yield the most intense excitation around 500 nm (2.48 eV, PBE functional) and 450 nm (2.76 eV, PBE0), and assign it to a dipole-allowed, z-polarized L-δ_g → f-δ_u* transition. The calculations therefore support the assignment of the experimental absorption feature at 545 nm (2.27 eV) when considering that previous calculations for $M(COT)_2$ also deviated from experimental UV-vis absorption energies by up to ca. 0.5 eV (*19*). LMCT states calculated near the observed band at 700 nm are assigned to L-δ_u → f-δ_u* transitions, with small oscillator strengths because of the parity selection rule; the increased intensity observed experimentally for these transitions may arise from vibronic coupling, which was not accounted for in the calculations.

The CAS calculations reveal that the ground state for both D_{2d}-$Bk(hdcCOT)_2$ and the unsubstituted D_{8h}-$Bk(COT)_2$ is dominated (87 weight-%) by the $(COT\text{-}\delta_g)^4(COT\text{-}\delta_u)^4f^7d^0$ configuration. The natural orbitals (Fig. 3B) exhibit metal-ligand hybridization. Similar to previous spectroscopic and theoretical studies of bonding in early actinide sandwich complexes (*50*), metal-ligand covalency in D_{2d}-$Bk(hdcCOT)_2$ occurs primarily in the doubly degenerate L-δ_u and L-δ_g orbitals (Fig. 3B), which have considerable metal weights (22% 5f and 26% 6d, respectively). The *same* wavefunction can alternatively be expressed by using ligand- vs. metal-localized linear combinations of the bonding-antibonding δ_u/δ_u* pairs, in which case the covalent ligand-to-5f donation appears primarily via admixture of charge-transfer configurations. This results in 70% weight of the Bk^{4+} configuration for D_{8h}-$Bk(COT)_2$ and D_{2d}-$Bk(hdcCOT)_2$ (Fig. 3C and Fig. S1D), indicating that both are meaningfully assigned as formally Bk^{4+}. Figure 3C presents the compositions of the ground state wavefunctions for D_{8h}-$An(COT)_2$ with An = Th–Bk when expressed in the aforementioned localized orbital set, in terms of the metal oxidation state. A sharp decrease in weight of the +3 configuration occurs between Cm (98%) and Bk (33%), which is reflective of a decrease in net donation from the ligands into the 5f-shell as both systems increase the relative weight of the stability and chemical inertness of the $5f^7$ configuration.

To understand how the stability of a half-filled, $5f^7$ shell may lead to a greater weight of the Bk^{4+} configuration, $Bk(hdcCOT)_2$ was compared to its Ce and Tb analogs. $Tb(COT)_2$ has not been observed experimentally, but was described in earlier theoretical work as having a ground state dominated by an 89% weight of the ionic $(L\text{-}\delta_g)^4(L\text{-}\delta_u)^3f^8d^0$ configuration, corresponding to Tb^{3+} (*48, 49*). This can be attributed to the large 4th ionization energy of Tb, which is similar to that of Cm (*44, 45*), such that the Tb^{4+} $4f^7$ configuration is comparatively high in energy and not sufficiently stabilized by COT^{2-} ligands. In contrast, the overlap between 5f and ligand orbitals that is evident in the natural orbitals for $Bk(hdcCOT)_2$ (Fig. 3B) must have a stabilizing effect on the Bk^{4+} ground state. A substantial degree of 4f-shell bonding is also apparent in the natural orbitals for $Ce(hdcCOT)_2$ and $Ce(COT)_2$; however, significant charge transfer into formally empty 4f orbitals (in contrast to the partially filled 5f orbitals in the Bk case) means these complexes have dominant Ce^{3+} character (Fig. 3C). The electron populations associated with the pairs of metal-COT - localized δ_u orbitals are $(L\text{-}\delta_u)^{3.67}(f\text{-}\delta_u)^{2.33}$ and $(L\text{-}\delta_u)^{3.15}(f\text{-}\delta_u)^{0.85}$ for $Bk(hdcCOT)_2$ and $Ce(hdcCOT)_2$, respectively. This suggests that the extent of ligand-to-metal donation is far more pronounced with Ce 4f-δ_u (0.85 electrons) than with Bk 5f-δ_u (0.33 electrons), i.e. the berkelocene has a dominant 4+ character.

Conclusions

The discovery and structural characterization of $Bk(hdcCOT)_2$ shows that Bk^{4+}–C bonds can be

stabilized in high valent Bk organometallics and how organometallic complexes of rare and radioactive isotopes can be obtained with less than 0.5 mg of metal. The new experimental data provides an opportunity to test electronic structure models across both the lanthanide and actinide series. The stark differences with its Ce^{4+} and Tb^{4+} analogs are peculiar, given that Ce^{4+} and Bk^{4+} have similar reduction potentials, and Tb^{4+} and Bk^{4+} both have half-filled f-shells. However, the half-filled Bk^{4+}-$5f^7$ configuration is uniquely stabilized by the productive metal–ligand overlap afforded by more radially-extended 5f orbitals.

Acknowledgments

Funding: This work was supported by the Director, Office of Science, Office of Basic Energy Sciences, Division of Chemical Sciences, Geosciences, and Biosciences Heavy Element Chemistry Program of the U.S. Department of Energy (DOE) at LBNL under Contract No. DE-AC02-05CH11231. J.Au. acknowledges support for the theoretical component of this study from the U.S. Department of Energy, Office of Basic Energy Sciences, Division of Chemical Sciences, Geosciences, and Biosciences, Heavy Element Chemistry Program, under grant DE-SC0001136. We thank the Center for Computational Research (CCR) at the University of Buffalo for providing computational resources. DCS acknowledges the computing infrastructure provided by the RECENT AIR grant agreement MySMIS no. 127324. J.A.B. and S.N.K. acknowledge support from a Department of Energy (DOE) Integrated University Program Fellowship at the University of California, Berkeley. This research used resources of the Advanced Light Source, which is a DOE Office of Science User Facility under Contract no. DE-AC02-05CH11231. We acknowledge Prof. T. Albrecht for providing a fraction of a $^{249}BkCl_3$ stock initially supplied by the National Isotope Development Center, which is managed by the DOE Isotope Program.

Author contributions: Conceptualization and Writing – original draft: D.R.R., A.N.G., A.N.P., D.-C.S., R.J.A., P.L.A., J.Au., and S.G.M. Formal Analysis: D.R.R., A.N.G., A.N.P., D.-C.S., X.Y., S.N.K., E.T.O., S.J.T., J.Au., and S.G.M. Funding acquisition: J.Ar., J.R.L., W.W.L., R.J.A., P.L.A., J.Au., S.G.M. Investigation: D.R.R., A.N.G., A.N.P., D.-C.S., J.N.W., N.K., A.A.P., J.A.B., X.Y., S.N.K., and E.T.O. Methodology: D.R.R., A.N.G., A.N.P., D.-C.S., J.W., and N.K. Project Administration: D.R.R., A.N.G., J.N.W., W.W.L., R.J.A., P.L.A., J.Au., and S.G.M. Resources: W.W.L, S.J.T., R.J.A., P.L.A., J.Au., and S.G.M. Supervision: J.Ar., J.R.L., W.W.L., S.J.T., R.J.A., P.L.A., J.Au., and S.G.M. Validation: D.R.R., A.N.G., A.N.P., A.A.P., J.N.W., J.A.B., S.J.T. Writing – reviewing and editing: all authors.

Competing interests: None.

Data and materials availability: All data are available in the main text or the supplementary materials.

References

1. G. Wilkinson, M. Rosenblum, M. C. Whiting, R. B. Woodward, The structure of iron bis-cyclopentadienyl. *J. Am. Chem. Soc.* **74**, 2125-2126 (1952).
2. E. O. Fischer, W. Pfab, Cyclopentadien-Metallkomplexe, ein neuer Typ metallorganischer Verbindgen. *Z. Naturforsch., B* **7**, 377-379 (1952).
3. S. G. Thompson, A. Ghiorso, G. T. Seaborg, The New Element Berkelium (Atomic Number 97). *Phys. Rev.* **80**, 781-789 (1950).

4. S. G. Thompson, K. Street, A. Ghiorso, G. T. Seaborg, The New Element Californium (Atomic Number 98). *Phys. Rev.* **80**, 790-796 (1950).
5. L. T. Reynolds, G. Wilkinson, π-Cyclopentadienyl Compounds of Uranium-IV and Thorium-IV. *J. Inorg. Nucl. Chem.* **2**, 246-253 (1956).
6. H. Gilman *et al.*, Organic Compounds of Uranium. I. 1,3-Dicarbonyl Chelates. *J. Am. Chem. Soc.* **78**, 2790-2792 (1956).
7. A. J. Streitwieser, U. Mueller-Westerhoff, Bis(cyclooctatetraenyl)uranium (uranocene). A new class of sandwich complexes that utilize atomic f orbitals. *J. Am. Chem. Soc.* **90**, 7364-7364 (1968).
8. A. Zalkin, K. N. Raymond, The Structure of Di-π-cyclooctatetraeneuranium (Uranocene). *J. Am. Chem. Soc.* **91**, 5667-& (1969).
9. A. J. Streitwieser, N. Yoshida, Di-π-cyclooctatetraenethorium. *J. Am. Chem. Soc.* **91**, 7528-7528 (1969).
10. D. G. Karraker, J. A. Stone, E. R. J. Jones, N. Edelstein, Bis(cyclooctatetraenyl)neptunium(IV) and bis(cyclooctatetraenyl)plutonium(IV). *J. Am. Chem. Soc.* **92**, 4841-4845 (1970).
11. D. F. Starks, T. C. Parsons, A. Streitwieser, N. Edelstein, Bis(π-cyclooctatetraene)protactinium. *Inorg. Chem.* **13**, 1307-1308 (1974).
12. A. Greco, S. Cesca, W. Bertolini, New π-Cyclooctatetranyl and π-Cyclopentadienyl Complexes of Cerium. *J. Organomet. Chem.* **113**, 321-330 (1976).
13. P. G. Laubereau, J. H. Burns, Microchemical preparation of tricyclopentadienyl compounds of berkelium, californium, and some lanthanide elements. *Inorg. Chem.* **9**, 1091-1095 (1970).
14. P. G. Laubereau, J. H. Burns, Tricyclopentadienyl-curium. *Inorg. Nucl. Chem. Lett.* **6**, 59-63 (1970).
15. C. A. P. Goodwin *et al.*, $[Am(C_5Me_5H)_3]$: An Organometallic Americium Complex. *Angew. Chem. Int. Ed.* **58**, 11695-11699 (2019).
16. C. A. P. Goodwin *et al.*, Isolation and characterization of a californium metallocene. *Nature* **599**, 421-424 (2021).
17. J. G. Brennan, J. C. Green, C. M. Redfern, Covalency in bis([8]annulene)uranium from photoelectron spectroscopy with variable photon energy. *J. Am. Chem. Soc.* **111**, 2373-2377 (1989).
18. M. Pepper, B. E. Bursten, The electronic structure of actinide-containing molecules: a challenge to applied quantum chemistry. *Chem. Rev.* **91**, 719-741 (1991).
19. A. Kerridge, N. Kaltsoyannis, Are the Ground States of the Later Actinocenes Multiconfigurational? All-Electron Spin-Orbit Coupled CASPT2 Calculations on $An(\eta^8\text{-}C_8H_8)_2$ (An = Th, U, Pu, Cm). *J. Phys. Chem. A* **113**, 8737-8745 (2009).
20. M. L. Neidig, D. L. Clark, R. L. Martin, Covalency in f-element complexes. *Coord. Chem. Rev.* **257**, 394-406 (2013).
21. S. G. Minasian *et al.*, New evidence for 5f covalency in actinocenes determined from carbon K-edge XAS and electronic structure theory. *Chem. Sci.* **5**, 351-359 (2014).
22. G. Ganguly, D.-C. Sergentu, J. Autschbach, Ab Initio Analysis of Metal–Ligand Bonding in $An(COT)_2$ with An=Th, U in Their Ground- and Core-Excited States. *Chem.-Eur. J.* **26**, 1776-1788 (2020).
23. A. N. Gaiser *et al.*, Creation of an unexpected plane of enhanced covalency in cerium(III) and berkelium(III) terpyridyl complexes. *Nat. Commun.* **12**, 7230 (2021).

24. S. Galley *et al.*, Synthesis and Characterization of Tris-chelate Complexes for Understanding f-Orbital Bonding in Later Actinides. *J. Am. Chem. Soc.* **141**, 2356-2366 (2019).
25. M. A. Silver *et al.*, Electronic Structure and Properties of Berkelium Iodates. *J. Am. Chem. Soc.* **139**, 13361-13375 (2017).
26. D. E. Hobart, J. R. Peterson, in *The Chemistry of the Actinide and Transactinide Elements,* L. Morss, N. Edelstein, J. Fuger, Eds. (Springer, Berlin, 2006), vol. 3, chap. 10, pp. 1444-1498.
27. S. G. Thompson, B. B. Cunningham, G. T. Seaborg, Chemical Properties of Berkelium. *J. Am. Chem. Soc.* **72**, 2798-2801 (1950).
28. M. R. Antonio, C. W. Williams, L. Soderholm, Berkelium redox speciation. *Radiochim. Acta* **90**, 851-856 (2002).
29. J. R. Stokely, R. D. Baybarz, J. R. Peterson, The formal potential of the Bk(IV)-Bk(III) couple in several media. *J. Inorg. Nucl. Chem.* **34**, 392-393 (1972).
30. E. Wadsworth, F. R. Duke, C. A. Goetz, Present Status of Cerium(IV)-Cerium(III) Potentials. *Anal. Chem.* **29**, 1824-1825 (1957).
31. M. Hiller, M. Maier, H. Wadepohl, M. Enders, Paramagnetic NMR Analysis of Substituted Biscyclooctatetraene Lanthanide Complexes. *Organometallics* **35**, 1916-1922 (2016).
32. J. D. Hilgar, A. K. Butts, J. D. Rinehart, A method for extending AC susceptometry to long-timescale magnetic relaxation. *Phys. Chem. Chem. Phys.* **21**, 22302-22307 (2019).
33. A. Streitwieser, S. A. Kinsley, C. H. Jenson, J. T. Rigsbee, Synthesis and Properties of Di-π-[8]annulenecerium(IV), Cerocene. *Organometallics* **23**, 5169-5175 (2004).
34. U. Kilimann, R. Herbst-Irmer, D. Stalke, F. T. Edelmann, An Efficient Access to Organocerium(IV) Complexes: Synthesis and Structure of Bis[1,3,6-tris(trimethylsilyl)cyclooctatetraene]cerium(IV). *Angew. Chem. Int. Ed.* **33**, 1618-1621 (1994).
35. D. R. Russo *et al.*, Synthesis and Structure of hdcCOT$_2$An (An = Th, U, Np Pu). *to be submitted*.
36. K. O. Hodgson, K. N. Raymond, Rotomeric configurations of a methyl-substituted cyclooctatetraene dianion complex of uranium(IV). Crystal and molecular structure of bis(1,3,5,7-tetramethylcyclooctatetraenyl)uranium(IV), U($C_8H_4(CH_3)_4$)$_2$. *Inorg. Chem.* **12**, 458-466 (1973).
37. A. Zalkin, D. H. Templeton, S. R. Berryhill, W. D. Luke, Crystal and Molecular Structure of bis[π-(cyclobutenocyclooctatetraene)]uranium(IV), U[$C_8H_6(CH_2)_2$]$_2$. *Inorg. Chem.* **18**, 2287-2289 (1979).
38. A. Zalkin, D. H. Templeton, W. D. Luke, A. J. Streitwieser, Synthesis and structure of dicyclopentenouranocene, U[$C_8H_6(CH_2)_3$]$_2$. *Organometallics* **1**, 618-622 (1982).
39. A. Avdeef, A. Zalkin, K. N. Raymond, K. O. Hodgson, Two Isostructural Actinide π Complexes. The Crystal and Molecular Structure of Bis(cyclooctatetraenyl)uranium(IV), U(C_8H_8)$_2$, and Bis(cyclooctatetraenyl)thorium(IV), Th(C_8H_8)$_2$. *Inorg. Chem.* **11**, 1083-& (1972).
40. D. J. A. De Ridder, J. Rebizant, C. Apostolidis, B. Kanellakopulos, E. Dornberger, Bis(cyclooctatetraenyl)neptunium(IV). *Acta Cryst. C* **52**, 597-600 (1996).

41. C. J. Windorff *et al.*, A Single Small-Scale Plutonium Redox Reaction System Yields Three Crystallographically-Characterizable Organoplutonium Complexes. *Inorg. Chem.* **59**, 13301-13314 (2020).
42. K. N. Raymond, C. W. J. Eigenbrot, Structural criteria for the mode of bonding of organoactinides and -lanthanides and related compounds. *Acc. Chem. Res.* **13**, 276-283 (1980).
43. F. Ferraro, C. A. Barboza, R. Arratia-Pérez, A Relativistic Study of the Electronic and Magnetic Properties of Cerocene and Thorocene and Its Anions. *J. Phys. Chem. A* **116**, 4170-4175 (2012).
44. X. Cao, M. Dolg, Segmented contraction scheme for small-core lanthanide pseudopotential basis sets. *J. Mol. Struct. (THEOCHEM)* **581**, 139-147 (2002).
45. X. Y. Cao, M. Dolg, Segmented contraction scheme for small-core actinide pseudopotential basis sets. *J. Mol. Struct. (THEOCHEM)* **673**, 203-209 (2004).
46. G. J.-P. Deblonde *et al.*, Chelation and stabilization of berkelium in oxidation state +IV. *Nat. Chem.* **9**, 843-849 (2017).
47. T. Nishiuchi *et al.*, Optical nature of non-substituted triphenylmethyl cation: Crystalline state emission, thermochromism, and phosphorescence. *Aggregate* **2**, e126 (2021).
48. W. J. Liu, M. Dolg, P. Fulde, Calculated properties of lanthanocene anions and the unusual electronic structure of their neutral counterparts. *Inorg. Chem.* **37**, 1067-1072 (1998).
49. W. J. Liu, M. Dolg, P. Fulde, Low-lying electronic states of lanthanocenes and actinocenes $M(C_8H_8)_2$ (M=Nd, Tb, Yb, U). *J. Chem. Phys.* **107**, 3584-3591 (1997).
50. A. H. H. Chang, R. M. Pitzer, Electronic structure and spectra of uranocene. *J. Am. Chem. Soc.* **111**, 2500-2507 (1989).